



Study of hadronic events and measurements of α_s between 30 and 91 GeV

M. Acciarri, O. Adriani, M. Aguilar-Benitez, S. Ahlen, J. Alcaraz, G. Alemani, J. Allaby, A. Aloisio, G. Alverson, M G. Alviggi, et al.

► To cite this version:

M. Acciarri, O. Adriani, M. Aguilar-Benitez, S. Ahlen, J. Alcaraz, et al.. Study of hadronic events and measurements of α_s between 30 and 91 GeV. Physics Letters B, 1997, 411, pp.339-353. 10.1016/S0370-2693(97)01000-9 . in2p3-00000260

HAL Id: in2p3-00000260

<https://hal.in2p3.fr/in2p3-00000260>

Submitted on 30 Nov 1998

HAL is a multi-disciplinary open access archive for the deposit and dissemination of scientific research documents, whether they are published or not. The documents may come from teaching and research institutions in France or abroad, or from public or private research centers.

L'archive ouverte pluridisciplinaire **HAL**, est destinée au dépôt et à la diffusion de documents scientifiques de niveau recherche, publiés ou non, émanant des établissements d'enseignement et de recherche français ou étrangers, des laboratoires publics ou privés.

Study of Hadronic Events and Measurements of α_s between 30 and 91 GeV

L3 Collaboration

Abstract

We have studied the structure of hadronic events with a hard, isolated photon in the final state ($e^+e^- \rightarrow Z \rightarrow \text{hadrons} + \gamma$) in the 3.6 million hadronic events collected with the L3 detector at centre-of-mass energies around 91 GeV. The centre-of-mass energy of the hadronic system is in the range 30 GeV to 86 GeV. Event shape variables have been measured at these reduced centre-of-mass energies and have been compared with the predictions of different QCD Monte Carlo programs. The event shape variables and the energy dependence of their mean values are well reproduced by QCD models. We fit distributions of several global event shape variables to resummed $\mathcal{O}(\alpha_s^2)$ calculations to determine the strong coupling constant α_s over a wide range of energies. We find that the strong coupling constant α_s decreases with increasing energy, as expected from QCD.

Submitted to *Phys. Lett. B*

1 Introduction

The study of events with high energy isolated photons in hadronic Z decays offers an important probe of the short distance structure of QCD [1]. The high energy photons are radiated early in the process either through initial-state radiation or through quark bremsstrahlung. On the other hand, the development of the hadronic shower takes place over a longer time scale. So a study of the recoiling hadronic system in events containing hard, isolated photon radiation gives access to hadron production at reduced centre-of-mass energies.

At LEP, with centre-of-mass energies (\sqrt{s}) around the Z mass, initial-state radiation (ISR) and interference between initial and final-state radiation (FSR) are highly suppressed. Selection of hadronic events with high energy isolated photons ensures a pure sample containing predominantly final-state radiation photons, with a small background from neutral hadron decays into photons.

We report here the results of such an analysis of hadronic Z decays at LEP collected with the L3 detector [2, 3]. The measured distributions are compared with event generators based on an improved leading log approximation (Parton Shower models including QCD coherence effects). Three such Monte Carlo programs, ARIADNE 4.06 [4], HERWIG 5.8 [5] and JETSET 7.4 PS [6], have been used for these comparisons. These programs differ in the variables used to define the parton shower evolution and also in the modelling of the hadronisation effects.

The measured distributions of event shape variables at the different reduced centre-of-mass energies have also been compared with the predictions of a second-order QCD calculation with resummed leading and next-to-leading terms. This provides determinations of the strong coupling constant α_s at several centre-of-mass energies. In addition, we use our measurements of α_s from similar analyses at $\sqrt{s} = 91$ GeV [7], 133 GeV [8], 161 GeV and 172 GeV [9] to study the energy evolution of α_s .

2 Event Selection

The events used in this study have been collected during LEP running from 1991 to 1995. The corresponding integrated luminosity is 142.4 pb^{-1} . The bulk of the data ($\simeq 107 \text{ pb}^{-1}$) corresponds to runs at $\sqrt{s} \simeq 91.2$ GeV, and the remaining part comes from runs during the LEP energy scans ($\sqrt{s} = 88$ to 93 GeV).

Hadronic events are recorded primarily by a calorimetric energy trigger with an efficiency exceeding 99.9%. The selection of events of the type $e^+e^- \rightarrow \text{hadrons}$ is based on the energy measurements in the electromagnetic calorimeter composed of BGO crystals and in the uranium hadron calorimeter with proportional wire chamber readout. Events are accepted if

$$0.6 \leq \frac{E_{\text{vis}}}{\sqrt{s}} \leq 1.4 \quad , \quad \frac{|E_{\parallel}|}{E_{\text{vis}}} \leq 0.40 \quad , \quad \frac{|E_{\perp}|}{E_{\text{vis}}} \leq 0.40 \quad , \quad N_{\text{cluster}} > 12$$

where E_{vis} is the total energy observed in the calorimeters; E_{\parallel} , E_{\perp} are respectively the energy imbalances along and transverse to the beam direction and N_{cluster} is the number of clusters with energy larger than 100 MeV. With these cuts, a total of 3.578 million hadronic events is selected from the entire data sample.

Monte Carlo hadronic events are generated by the parton shower program JETSET and passed through the L3 detector simulation [10]. The above selection cuts accept 98% of the simulated hadronic events, with a small background of 0.2% from $\tau^+\tau^-$ and two-photon collision processes.

While jets are reconstructed using the hadron calorimeter which has a polar angular acceptance $5^\circ < \theta < 175^\circ$, photon candidates are detected in the solid angle covered by the barrel and end-cap electromagnetic calorimeters ($11.6^\circ < \theta < 36^\circ$, $42^\circ < \theta < 138^\circ$, $144^\circ < \theta < 168.4^\circ$). A loose pre-selection of photon candidates according to the following criteria is applied to the hadronic data sample. A cluster in the electromagnetic calorimeter is considered to be an energetic, isolated photon candidate if

- its energy is larger than 5 GeV.
- there is no charged track associated with it. Tracks are selected by requiring at least 20 hits in the tracking chamber and a transverse momentum greater than 50 MeV. For tracks in the end-cap region, the requirement on the minimum number of hits is changed to two-thirds of the number of wires between the first and last recorded hits.
- the lateral shower profile is consistent with that of a photon and the cluster is isolated, that is, no other cluster with energy ($E_{\alpha_{\text{LI}}}$) above 250 MeV is found in a cone of half-angle (α_{LI}) 10° around the candidate direction.

A total of 126 046 events is selected by these criteria. The photon energy (E_γ) is related to the centre-of-mass energy of the recoiling hadronic system ($\sqrt{s'}$) by :

$$\sqrt{s'} = \sqrt{s \left(1 - \frac{2E_\gamma}{\sqrt{s}} \right)}.$$

We have studied whether $\sqrt{s'}$ is the correct scale of hadron production by comparing Monte Carlo hadronic Z decay events containing isolated final-state photons with Monte Carlo e^+e^- interactions without initial and final-state radiation, but with the same hadronic centre-of-mass energy. The distributions of event shape variables studied are found to be very similar for these two sets of events. This suggests that $\sqrt{s'}$ can be used as the QCD scale. Effects from late photon radiation off quarks and hadrons are suppressed by the high energy requirement and strict isolation of the photon, as described below. We divide the $\sqrt{s'}$ spectrum into six regions. The energy regions and the corresponding numbers of pre-selected events are summarised in table 1.

The background to the direct photons is dominated by photons from π^0 and η decays. To reduce this background, we require that the shower be isolated and its shape be compatible with the electromagnetic shower of a single photon. A shower shape discriminator ϵ_γ , based on an artificial neural network [11], is used to distinguish multi-photon showers from single-photon ones in the electromagnetic calorimeter. The cut values for the following parameters are tuned separately for the six $\sqrt{s'}$ ranges by optimising the efficiency and the purity at each energy :

- the neural network probability, ϵ_γ ,
- the size of the local isolation cone, α_{LI} ,
- the angle to the nearest jet, α_{JI} (reconstructed from the recoiling hadronic system using the JADE algorithm [12] with $y_{\text{cut}} = 0.05$),
- the minimum energy of individual clusters within the local isolation cone, $E_{\alpha_{\text{LI}}}$.

The purity of the photon signal and the efficiency of selection are optimised using 6.7 million JETSET parton shower events processed through the L3 detector simulation program. The isolation angles have been chosen to be energy dependent in order to get the best performance in the efficiency-purity plane. The energy cutoff $E_{\alpha_{LI}}$ is tightened to 50 MeV for all energy points, and the cut on the neural network discriminator is chosen to keep 85% of photons passing all other cuts. Photons are selected from ISR or FSR with an efficiency between 27.4% and 48.3% depending on their energies, giving a purity of better than 68.4% at all energies. The cuts, as well as the number of events, are summarised in table 1.

The important sources of remaining background are misidentified hadrons and photons from hadron decays. This has been studied using the JETSET PS Monte Carlo events with complete detector simulation. As observed in our earlier studies [13], the absolute rate of the background is not well described in the Monte Carlo. The latter has, therefore, been estimated from the data by selecting a background sample with the same photon energy and isolation requirement, but a low probability ($\leq 5\%$) of the neural network discriminator. This sample is compared with the Monte Carlo sample assuming that the remaining signal part is well described. For JETSET, an overall normalisation factor between 1.2 ± 0.1 and 2.0 ± 0.1 is obtained, depending on the $\sqrt{s'}$ value. The estimated background content has been varied by one standard deviation to determine the systematic effect on the measured distributions due to the above assumption. The background scale factors have also been estimated with the HERWIG Monte Carlo event sample; these scale factors agree with those obtained from JETSET within their errors. Backgrounds due to $\tau^+\tau^-$ and two-photon events have been calculated using Monte Carlo [14] event samples normalised to the total integrated luminosity. The level of backgrounds in the six energy regions are also summarised in table 1.

3 Global Event Shape Variables

Event shape variables are calculated after boosting the event to the centre-of-mass frame of the recoiling hadronic system using the well-measured energy and angle of the isolated photon. The variables studied are event thrust (T) [15], scaled heavy jet mass (ρ) [16] and total (B_T) and wide (B_W) jet broadenings [17]. The jet broadening variables are defined by dividing the event into two hemispheres (S_{\pm}) by a plane perpendicular to the thrust axis \vec{n}_T and then computing the quantities

$$B_{\pm} = \frac{\sum_{i \in S_{\pm}} |\vec{p}_i \times \vec{n}_T|}{2 \sum_i |\vec{p}_i|}.$$

The variables B_T and B_W are then defined as,

$$B_T = B_+ + B_- \quad \text{and} \quad B_W = \max(B_+, B_-).$$

Figures 1(a-f) show the measured thrust distributions for the six $\sqrt{s'}$ ranges together with the Monte Carlo predictions. The different shaded areas indicate the backgrounds from fragmentation in the hadronic sample, $\tau^+\tau^-$ and two-photon processes. The Monte Carlo expectations agree with the measured distributions (in these comparisons, the hadronic background has been rescaled). Similar behaviour is observed in all the measured distributions. For the comparison with the QCD models and the fits to α_s described below, the backgrounds are subtracted bin by bin.

The effect of the detector resolution has been studied by comparing the event shape variables of accepted JETSET Monte Carlo events before and after detector simulation. Data are also

corrected for detector acceptance using the JETSET Monte Carlo program. All corrections are applied bin by bin and they are typically less than 20%.

The systematic errors in the distributions of event shape variables arise mainly due to uncertainties in detector calibration, in corrections for detector effects and in estimating the background contamination. The effect of detector calibration and inhomogeneities has been studied by:

- changing the definition of reconstructed objects used in the detector to calculate the observables. Instead of using only calorimetric clusters, the analysis has been repeated with objects obtained from a non-linear combination of energies of charged tracks and calorimetric clusters.
- restricting the analysis to an event sample where the isolated photon is detected in the central part of the detector ($|\cos\theta_\gamma| < 0.73$).
- using different Monte Carlo samples in correcting the data. We have used two sets of Monte Carlo samples generated using JETSET and HERWIG.

The systematic errors arising from background subtraction are estimated by:

- varying the background scale factors by one standard deviation. The bin-by-bin systematic errors are less than 4%.
- varying the cuts on the neural network probability, the jet and local isolation angles, and the energy in the local isolation cone. The bin-by-bin systematic errors are 3–5%.

The final systematic error is taken as the sum in quadrature of all the above mentioned contributions. The bin-by-bin systematic errors are typically 18%, comparable to the statistical error.

4 Comparison with QCD Models

Figures 2(a-f) show the corrected, background-subtracted distributions for the total jet broadening (B_T) for the six $\sqrt{s'}$ ranges. These distributions are compared with predictions from ARIADNE [4], HERWIG [5] and JETSET [6]. The Monte Carlo events are generated using a set of parameters tuned using the data taken on the Z peak [18]. Initial and final-state radiation has been switched off and the beam energy corresponds to the reduced centre-of-mass energy distribution of the observed data sample. The same flavour composition is used as in the radiative Z decays. As can be seen in figure 2, the QCD model predictions are in good agreement with the data. This is also the case for the other event shape variables studied.

The measured mean values of thrust, scaled heavy jet mass, and total and wide jet broadenings at the different reduced centre-of-mass energies are summarised in table 2. Figure 3 shows the energy evolution of these mean values. We also include the L3 measurements of these parameters at $\sqrt{s} = m_Z$ [7, 19], 133 GeV [8], 161 GeV and 172 GeV [9]. The energy evolution of these variables are compared with different QCD models and the predictions from the different parton shower models agree with the trend in the data.

5 Determination of α_s

QCD predictions in fixed second-order perturbation theory [20,21] do not take into account the effect of multiple gluon emission. For variables like thrust, heavy jet mass, etc. the fixed-order predictions become unreliable in kinematic regions where multi-gluon emission is important, and the associated leading and sub-leading large logarithmic terms require resummation. Such calculations have been carried out for the variables $1 - T$, ρ , B_T , B_W (denoted generically by y) to next-to-leading log terms [17,22,23]. In order to describe the data over a wide kinematic range, it is desirable to combine the two sets of calculations taking into account their common parts. A number of different ‘matching schemes’ have been proposed to avoid double counting of terms from the fixed-order and resummed pieces of the calculation. In addition, the kinematic constraints have to be satisfied, that is, the cross sections vanish beyond the kinematic limits. This can be achieved by replacing the variable y in the resummed terms by $(y^{-1} - y_{\max}^{-1} + 1)^{-1}$ [24]. These calculations are done for partons and do not include heavy quark mass effects.

To compare the analytical calculations with the experimental distributions, a correction is applied for the effect of hadronisation and decays, using Monte Carlo programs. We have used the parton shower programs JETSET, ARIADNE and HERWIG with string or cluster fragmentation.

We compare the resulting differential cross section to our measurements. The correction for hadronisation and decays changes the perturbative prediction by less than 10% for the event shape variables over a large kinematic range. The correction increases in the extreme two-jet region.

In order to measure α_s , we fit the theoretical distributions to our measured event shape distributions for a fixed scale $\mu = \sqrt{s'}$. For the fit we use the ranges of the values of the variables as given in table 3. The choice of these ranges is determined by the reliability of the resummation calculation, the size and uniformity of corrections for detector and hadronisation effects, and sufficient statistics.

Figures 4(a-f) show the experimental data, together with the QCD fits, for the scaled heavy jet mass at the six reduced centre-of-mass energies. The results in table 4 are the α_s values at two typical reduced centre-of-mass energies as obtained from the fits to $\mathcal{O}(\alpha_s^2)$ plus resummed calculations using hadronisation corrections from JETSET, together with the χ^2 values.

The errors shown in table 4 are divided into three main parts. The first corresponds to the statistical errors, together with the experimental systematic uncertainties estimated by changing the background scale factors, selection cuts and correction procedures. The overall experimental error is obtained by adding the statistical and systematic errors in quadrature. The second part shows the variation in the fitted value of α_s when hadronisation corrections were calculated using HERWIG or ARIADNE instead of JETSET (fragmentation model), or when the fragmentation parameters within JETSET were varied (model parameters). For all variables, the most important variation comes from the different fragmentation models, so we use this as an estimate of the overall hadronisation uncertainty. The third part summarises the errors coming from uncalculated higher orders in the QCD predictions. The scale error is obtained by repeating the α_s fit for different values of the renormalisation scale in the interval $0.5\sqrt{s'} \leq \mu \leq 2\sqrt{s'}$. For all these scales a good fit is obtained. The matching scheme uncertainty is obtained from half of the maximum spread due to the variation of the matching algorithm. The systematic errors due to uncalculated higher-order terms have been estimated independently from the scale uncertainty and the matching scheme uncertainty. The largest of these is taken as the theoretical uncertainty due to uncalculated higher orders. The overall

theoretical error is obtained by adding to this in quadrature, the hadronisation uncertainty.

The α_s values from the four distributions are affected differently by higher-order corrections and hadronisation effects. To obtain a combined value for the strong coupling constant, we take the unweighted average of the four α_s values at each centre-of-mass energy. The overall experimental error is obtained by adding in quadrature the statistical error and the unweighted average of experimental systematic errors. The overall theoretical uncertainty is estimated as the unweighted average of the theoretical errors obtained from the four different measurements at each centre-of-mass energy. The combined results are summarised in table 5.

We have compared the α_s values measured at the different centre-of-mass energies to those measured by L3 from similar analyses at $\sqrt{s} = m_Z$ [7], 133 GeV [8], 161 GeV and 172 GeV [9]. The most precise measurement of α_s comes from the determination at $\sqrt{s} = m_Z$ from the four event shape variables :

$$\alpha_s(m_Z) = 0.1221 \pm 0.0020 \pm 0.0066,$$

where the first error is experimental and the second error is theoretical. It should be noted that the theoretical errors are strongly correlated between these ten measurements. The higher-order uncertainties should be the same, and the uncertainties due to hadronisation corrections are comparable at these energies. The error, appropriate to a measurement of the energy dependence of α_s , can then be considered to be purely experimental.

The experimental systematic errors on α_s are dominated by the background uncertainties. These are similar for all the individual low-energy or high-energy data points, but differ between the low-energy, Z-peak and high-energy data sets. The experimental systematic errors are then different and uncorrelated between the three data sets, but are taken as fully correlated between individual low-energy or high-energy measurements. Table 6 summarises the α_s values from our measurements at the ten centre-of-mass energies, evaluated at the m_Z scale according to the QCD evolution equation in reference [25]. The ten measurements are shown in figure 5 with experimental errors only, together with a fit to the QCD evolution equation with $\alpha_s(m_Z)$ as a free parameter. The fit gives a χ^2 of 12.2 for nine degrees of freedom, corresponding to a confidence level of 0.20, with a fitted value of α_s :

$$\alpha_s(m_Z) = 0.1207 \pm 0.0016 \pm 0.0066.$$

On the other hand, a model with a constant α_s gives a χ^2 of 42.4 which corresponds to a confidence level of 0.3×10^{-5} .

Acknowledgements

We wish to express our gratitude to the CERN accelerator divisions for the excellent performance of the LEP accelerator. We acknowledge the contributions of all the engineers and technicians who have participated in the construction and maintenance of this experiment.

References

- [1] M. Gell-Mann, Acta Phys. Austriaca Suppl. **IX** (1972) 733;
H. Fritzsch and M. Gell-Mann, 16th International Conference on High Energy Physics, Batavia, 1972; editors J.D. Jackson and A. Roberts, National Accelerator Laboratory (1972);
H. Fritzsch, M. Gell-Mann and H. Leutwyler, Phys. Lett. **B47** (1973) 365;
D.J. Gross and F. Wilczek, Phys. Rev. Lett. **30** (1973) 1343;
D.J. Gross and F. Wilczek, Phys. Rev. **D8** (1973) 3633;
H.D. Politzer, Phys. Rev. Lett. **30** (1973) 1346;
G. 't Hooft, Nucl. Phys. **B33** (1971) 173.
- [2] L3 Collaboration, B. Adeva *et al.*, Nucl. Inst. Meth. **A289** (1990) 35;
M. Chemarin *et al.*, Nucl. Inst. Meth. **A349** (1994) 345;
M. Acciarri *et al.*, Nucl. Inst. Meth. **A351** (1994) 300;
G. Basti *et al.*, Nucl. Inst. Meth. **A374** (1996) 293;
A. Adam *et al.*, Nucl. Inst. Meth. **A383** (1996) 342.
- [3] L3 Collaboration, O. Adriani *et al.*, Phys. Rep., **236** (1993) 1.
- [4] ARIADNE 4.06 Monte Carlo Program:
U. Pettersson, “ARIADNE: A Monte Carlo for QCD Cascades in the Colour Dipole Formulation”, Lund Preprint, LU TP 88-5 (1988);
L. Lönnblad, “The Colour Dipole Cascade Model and the Ariadne Program”, Lund Preprint, LU TP 91-11 (1991).
- [5] HERWIG 5.8 Monte Carlo Program:
G. Marchesini and B. Webber, Nucl. Phys. **B310** (1988) 461;
I.G. Knowles, Nucl. Phys. **B310** (1988) 571;
G. Marchesini *et al.*, Comp. Phys. Comm. **67** (1992) 465.
- [6] JETSET 7.4 Monte Carlo Program:
T. Sjöstrand, Comp. Phys. Comm. **82** (1994) 74.
- [7] L3 Collaboration, O. Adriani *et al.*, Phys. Lett. **B284** (1992) 471;
S. Banerjee, S.Müller, L3 Internal Note No. 1441 (1993)¹⁾.
- [8] L3 Collaboration, M. Acciarri *et al.*, Phys. Lett. **B371** (1996) 137.
- [9] L3 Collaboration, M. Acciarri *et al.*, CERN-PPE/97-42.
- [10] The L3 detector simulation is based on GEANT Version 3.15.
See R. Brun *et al.*, “GEANT 3”, CERN DD/EE/84-1 (Revised), September 1987.
The GHEISHA program (H. Fesefeldt, RWTH Aachen Report PITHA 85/02 (1985)) is used to simulate hadronic interactions.
- [11] D. Kirkby, L3 Internal Note No. 1816 (1995)¹⁾;
D. Kirkby, “A Study of Final-State Radiation in Hadronic Z Decays”, Ph. D. Thesis, California Institute of Technology (1996), unpublished.
- [12] JADE Collaboration, W. Bartel *et al.*, Z. Phys. **C33** (1986) 23;
JADE Collaboration, S. Bethke *et al.*, Phys. Lett. **B213** (1988) 235.

- [13] L3 Collaboration, O. Adriani *et al.*, Phys. Lett. **B292** (1992) 472.
- [14] KORALZ 4.01 Monte Carlo Program is used for the $\tau^+\tau^-$ final state:
S. Jadach, B. F. L. Ward and Z. Was, Comp. Phys. Comm. **79** (1994), 503.
DIAG36 Monte Carlo program is used for two photon collision processes:
F. A. Berends, P. H. Daverveldt and R. Kleiss, Nucl. Phys. **B253** (1985) 441.
- [15] S. Brandt *et al.*, Phys. Lett. **12** (1964) 57;
E. Farhi, Phys. Rev. Lett. **39** (1977) 1587.
- [16] T. Chandramohan and L. Clavelli, Nucl. Phys. **B184** (1981) 365;
Mark II Collaboration, A. Peterson *et al.*, Phys. Rev. **D37** (1988) 1;
TASSO Collaboration, W. Braunschweig *et al.*, Z. Phys. **C45** (1989) 11.
- [17] S. Catani *et al.*, Phys. Lett. **B295** (1992) 269.
- [18] S. Banerjee, S. Banerjee, L3 Internal Note No. 1978 (1996). ¹⁾
- [19] L3 Collaboration, B. Adeva *et al.*, Z. Phys. **C55** (1992) 39.
- [20] R.K. Ellis, D.A. Ross and A.E. Terrano, Nucl. Phys. **B178** (1981) 421.
- [21] Z. Kunszt and P. Nason in “Z Physics at LEP 1”, CERN Report 89-08, Vol.I, p. 373.
- [22] S. Catani *et al.*, Phys. Lett. **B263** (1991) 491.
- [23] S. Catani *et al.*, Phys. Lett. **B272** (1991) 368.
- [24] S. Catani *et al.*, Nucl. Phys. **B407** (1993) 3.
- [25] Particle Data Group, R.M. Barnett *et al.*, Phys. Rev. **D54** (1996) 77.

¹⁾These L3 Internal Notes are available on request from: The L3 secretariat, CERN, CH-1211 Geneva 23, Switzerland.

The L3 Collaboration:

M. Acciarri,²⁸ O. Adriani,¹⁷ M. Aguilar-Benitez,²⁷ S. Ahlen,¹¹ J. Alcaraz,²⁷ G. Alemani,²³ J. Allaby,¹⁸ A. Aloisio,³⁰ G. Alverson,¹² M. G. Alvigi,³⁰ G. Ambrosi,²⁰ H. Anderhub,⁵⁰ V. P. Andreev,³⁹ T. Angelescu,¹³ F. Anselmo,⁹ A. Arefiev,²⁹ T. Azemoon,³ T. Aziz,¹⁰ P. Bagnaia,³⁸ L. Baksay,⁴⁵ R. C. Ball,³ S. Banerjee,¹⁰ Sw. Banerjee,¹⁰ K. Banicz,⁴⁷ A. Barczyk,^{50,48} R. Barillere,¹⁸ L. Barone,³⁸ P. Bartalini,³⁵ A. Baschirotto,²⁸ M. Basile,⁹ R. Battiston,³⁵ A. Bay,²³ F. Becattini,¹⁷ U. Becker,¹⁶ F. Behner,⁵⁰ J. Berdugo,²⁷ P. Berges,¹⁶ B. Bertucci,³⁵ B. L. Betev,⁵⁰ S. Bhattacharya,¹⁰ M. Biasini,¹⁸ A. Biland,⁵⁰ G. M. Bilei,³⁵ J. J. Blaising,⁴ S. C. Blyth,³⁶ G. J. Bobbink,² R. Bock,¹ A. Böhm,¹ L. Boldizsar,¹⁴ B. Borgia,³⁸ A. Boucham,⁴ D. Bourilkov,⁵⁰ M. Bourquin,²⁰ D. Boutigny,⁴ S. Braccini,²⁰ J. G. Branson,⁴¹ V. Brigljevic,⁵⁰ I. C. Brock,³⁶ A. Buffini,¹⁷ A. Buijs,⁴⁶ J. D. Burger,¹⁶ W. J. Burger,²⁰ J. Busenitz,⁴⁵ X. D. Cai,¹⁶ M. Campanelli,⁵⁰ M. Capell,¹⁶ G. Cara Romeo,⁹ G. Carlino,³⁰ A. M. Cartacci,¹⁷ J. Casaus,²⁷ G. Castellini,¹⁷ F. Cavallari,³⁸ N. Cavallo,³⁰ C. Cecchi,²⁰ M. Cerrada,²⁷ F. Cesaroni,²⁴ M. Chamizo,²⁷ Y. H. Chang,⁵² U. K. Chaturvedi,¹⁹ S. V. Chekanov,³² M. Chemarin,²⁶ A. Chen,⁵² G. Chen,⁷ G. M. Chen,⁷ H. F. Chen,²¹ H. S. Chen,⁷ M. Chen,¹⁶ G. Chiefari,³⁰ C. Y. Chien,⁵ L. Cifarelli,⁴⁰ F. Cindolo,⁹ C. Cividini,¹⁷ I. Clare,¹⁶ R. Clare,¹⁶ H. O. Cohn,³³ G. Coignet,⁴ A. P. Colijn,² N. Colino,²⁷ V. Commichau,¹ S. Costantini,⁸ F. Cotorobai,¹³ B. de la Cruz,²⁷ A. Csilling,¹⁴ T. S. Dai,¹⁶ R. D' Alessandro,¹⁷ R. de Asmundis,³⁰ A. Degré,⁴ K. Deiters,⁴⁸ P. Denes,³⁷ F. DeNotaristefani,³⁸ D. DiBitonto,⁴⁵ M. Diemoz,³⁸ D. van Dierendonck,² F. Di Lodovico,⁵⁰ C. Dionisi,³⁸ M. Dittmar,⁵⁰ A. Dominguez,⁴¹ A. Doria,³⁰ I. Dorne,⁴ M. T. Dova,^{19,4} E. Drago,³⁰ D. Duchesneau,⁴ P. Duinker,² I. Duran,⁴² S. Dutta,¹⁰ S. Easo,³⁵ Yu. Efremenko,³³ H. El Mamouni,²⁶ A. Engler,³⁶ F. J. Eppling,¹⁶ F. C. Erné,² J. P. Ernenwein,²⁶ P. Extermann,²⁰ M. Fabre,⁴⁸ R. Faccini,³⁸ S. Falciano,³⁸ A. Favara,¹⁷ J. Fay,²⁶ O. Fedin,³⁹ M. Felcini,⁵⁰ B. Fenyi,⁴⁵ T. Ferguson,³⁶ F. Ferroni,³⁸ H. Fesefeldt,¹ E. Fiandrini,³⁵ J. H. Field,²⁰ F. Filthaut,³⁶ P. H. Fisher,¹⁶ I. Fisk,⁴¹ G. Forconi,¹⁶ L. Fredj,²⁰ K. Freudenreich,⁵⁰ C. Furetta,²⁸ Yu. Galaktionov,^{29,16} S. N. Ganguli,¹⁰ P. Garcia-Abia,⁴⁹ S. S. Gau,¹² S. Gentile,³⁸ J. Gerald,⁵ N. Gheordanescu,¹³ S. Giagu,³⁸ S. Goldfarb,²³ J. Goldstein,¹¹ Z. F. Gong,²¹ A. Gougas,⁵ G. Gratta,³⁴ M. W. Gruenewald,⁸ V. K. Gupta,³⁷ A. Gurtu,¹⁰ L. J. Gutay,⁴⁷ B. Hartmann,¹ A. Hasan,³¹ D. Hatzifotiadiou,⁹ T. Hebbeker,⁸ A. Hervé,¹⁸ W. C. van Hoek,³² H. Hofer,⁵⁰ S. J. Hong,⁴⁴ H. Hoorani,³⁶ S. R. Hou,⁵² G. Hu,⁵ V. Innocente,¹⁸ H. Janssen,⁴ K. Jenkes,¹ B. N. Jin,⁷ L. W. Jones,³ P. de Jong,¹⁸ I. Josa-Mutuberria,²⁷ A. Kasser,²³ R. A. Khan,¹⁹ D. Kamrad,⁴⁹ Yu. Kamyshev,³³ J. S. Kapustinsky,²⁵ Y. Karyotakis,⁴ M. Kaur,^{19,4} M. N. Kienzle-Focacci,²⁰ D. Kim,³⁸ D. H. Kim,⁴⁴ J. K. Kim,⁴⁴ S. C. Kim,⁴⁴ Y. G. Kim,⁴⁴ W. W. Kinnison,²⁵ A. Kirkby,³⁴ D. Kirkby,³⁴ J. Kirkby,¹⁸ D. Kiss,¹⁴ W. Kittel,³² A. Klimentov,^{16,29} A. C. König,³² A. Kopp,⁴⁹ I. Korolko,²⁹ V. Koutsenko,^{16,29} R. W. Kraemer,³⁶ W. Krenz,¹ A. Kunin,^{16,29} P. Ladrón de Guevara,²⁷ G. Landi,¹⁷ C. Lapoint,¹⁶ K. Lassila-Perini,⁵⁰ P. Laurikainen,²² M. Lebeau,¹⁸ A. Lebedev,¹⁶ P. Lebrun,²⁶ P. Lecomte,⁵⁰ P. Lecoq,¹⁸ P. Le Coultre,⁵⁰ C. Leggett,³ J. M. Le Goff,¹⁸ R. Leiste,⁴⁹ E. Leonardi,³⁸ P. Levchenko,³⁹ C. Li,²¹ C. H. Lin,⁵² W. T. Lin,⁵² F. L. Linde,^{2,18} L. Lista,³⁰ Z. A. Liu,⁷ W. Lohmann,⁴⁹ E. Longo,³⁸ W. Lu,³⁴ Y. S. Lu,⁷ K. Lübelmeyer,¹ C. Luci,³⁸ D. Luckey,¹⁶ L. Luminari,³⁸ W. Lustermaier,⁴⁸ W. G. Ma,²¹ M. Maity,¹⁰ G. Majumder,¹⁰ L. Malgeri,³⁸ A. Malinin,²⁹ C. Mañá,²⁷ D. Mangle,³² S. Mangla,¹⁰ P. Marchesini,⁵⁰ A. Marin,¹¹ J. P. Martin,²⁶ F. Marzano,³⁸ G. G. Massaro,² D. McNally,¹⁸ S. Mele,³⁰ L. Merola,³⁰ M. Meschini,¹⁷ W. J. Metzger,³² M. von der Mey,¹ Y. Mi,²³ A. Mihul,¹³ A. J. W. van Mil,³² G. Mirabelli,³⁸ J. Mnich,¹⁸ P. Molnar,⁸ B. Monteleoni,¹⁷ R. Moore,³ S. Morganti,³⁸ T. Moulik,¹⁰ R. Mount,³⁴ S. Müller,¹ F. Muheim,²⁰ A. J. M. Muijs,² S. Nahn,¹⁶ M. Napolitano,³⁰ F. Nessi-Tedaldi,⁵⁰ H. Newman,³⁴ T. Niessen,¹ A. Nippe,¹ A. Nisati,³⁸ H. Nowak,⁴⁹ Y. D. Oh,⁴⁴ H. Opitz,¹ G. Organtini,³⁸ R. Ostonen,²² C. Palomares,²⁷ D. Pandoulas,¹ S. Paoletti,³⁸ P. Paolucci,³⁰ H. K. Park,³⁶ I. H. Park,⁴⁴ G. Pascale,³⁸ G. Passaleva,¹⁷ S. Patricelli,³⁰ T. Paul,¹² M. Pauluzzi,³⁵ C. Paus,¹ F. Pauss,⁵⁰ D. Peach,¹⁸ Y. J. Pei,¹ S. Pensotti,²⁸ D. Perret-Gallix,⁴ B. Petersen,³² S. Petrak,⁸ A. Pevsner,⁵ D. Piccolo,³⁰ M. Pieri,¹⁷ J. C. Pinto,³⁶ P. A. Piroué,³⁷ E. Pistolesi,²⁸ V. Plyaskin,²⁹ M. Pohl,⁵⁰ V. Pojidaev,^{29,17} H. Postema,¹⁶ N. Produit,²⁰ D. Prokofiev,³⁹ G. Rahal-Callot,⁵⁰ N. Raja,¹⁰ P. G. Rancoita,²⁸ M. Rattaggi,²⁸ G. Raven,⁴¹ P. Razis,³¹ K. Read,³³ D. Ren,⁵⁰ M. Rescigno,³⁸ S. Reucroft,¹² T. van Rhee,⁴⁶ S. Riemann,⁴⁹ K. Riles,³ O. Rind,³ A. Robohm,⁵⁰ J. Rodin,¹⁶ B. P. Roe,³ L. Romero,²⁷ S. Rosier-Lees,⁴ Ph. Rosset,²³ W. van Rossum,⁴⁶ S. Roth,¹ J. A. Rubio,¹⁸ D. Ruschmeier,⁸ H. Rykaczewski,⁵⁰ J. Salicio,¹⁸ E. Sanchez,²⁷ M. P. Sanders,³² M. E. Sarakinos,²² S. Sarkar,¹⁰ M. Sassowsky,¹ G. Sauvage,⁴ C. Schäfer,¹ V. Schegelsky,³⁹ S. Schmidt-Kaerst,¹ D. Schmitz,¹ P. Schmitz,¹ M. Schneegans,⁴ N. Scholz,⁵⁰ H. Schopper,⁵¹ D. J. Schotanus,³² J. Schwenke,¹ G. Schwering,¹ C. Sciacca,³⁰ D. Sciarrino,²⁰ L. Servoli,³⁵ S. Shevchenko,³⁴ N. Shivarov,⁴³ V. Shoutko,²⁹ J. Shukla,²⁵ E. Shumilov,²⁹ A. Shvorob,³⁴ T. Siedenburger,¹ D. Son,⁴⁴ A. Sopczak,⁴⁹ V. Soulimov,³⁰ B. Smith,¹⁶ P. Spillantini,¹⁷ M. Steuer,¹⁶ D. P. Stickland,³⁷ H. Stone,³⁷ B. Stoyanov,⁴³ A. Straessner,¹ K. Strauch,¹⁵ K. Sudhakar,¹⁰ G. Sultanov,¹⁹ L. Z. Sun,²¹ G. F. Susinno,²⁰ H. Suter,⁵⁰ J. D. Swain,¹⁹ X. W. Tang,⁷ L. Tauscher,⁴⁵ L. Taylor,¹² Samuel C. C. Ting,¹⁶ S. M. Ting,¹⁶ M. Tonutti,¹ S. C. Tonwar,¹⁰ J. Tóth,¹⁴ C. Tully,³⁷ H. Tuchscherer,⁴⁵ K. L. Tung,⁷ Y. Uchida,¹⁶ J. Ulbricht,⁵⁰ U. Uwer,¹⁸ E. Valente,³⁸ R. T. Van de Walle,³² G. Vesztegombi,¹⁴ I. Vetlitsky,²⁹ G. Viertel,⁵⁰ M. Vivargent,⁴ R. Völkert,⁴⁹ H. Vogel,³⁶ H. Vogt,⁴⁹ I. Vorobiev,²⁹ A. A. Vorobyov,³⁹ A. Vorvolakos,³¹ M. Wadhwa,⁵ W. Wallraff,¹ J. C. Wang,¹⁶ X. L. Wang,²¹ Z. M. Wang,²¹ A. Weber,¹ F. Wittgenstein,¹⁸ S. X. Wu,¹⁹ S. Wynhoff,¹ J. Xu,¹¹ Z. Z. Xu,²¹ B. Z. Yang,²¹ C. G. Yang,⁷ X. Y. Yao,⁷ J. B. Ye,²¹ S. C. Yeh,⁵² J. M. You,³⁶ An. Zalite,³⁹ Yu. Zalite,³⁹ P. Zemp,⁵⁰ Y. Zeng,¹ Z. Zhang,⁷ Z. P. Zhang,²¹ B. Zhou,¹¹ Y. Zhou,³ G. Y. Zhu,⁷ R. Y. Zhu,³⁴ A. Zichichi,^{9,18,19} F. Ziegler.⁴⁹

- 1 I. Physikalisches Institut, RWTH, D-52056 Aachen, FRG[§]
 - III. Physikalisches Institut, RWTH, D-52056 Aachen, FRG[§]
 - 2 National Institute for High Energy Physics, NIKHEF, and University of Amsterdam, NL-1009 DB Amsterdam, The Netherlands
 - 3 University of Michigan, Ann Arbor, MI 48109, USA
 - 4 Laboratoire d'Annecy-le-Vieux de Physique des Particules, LAPP, IN2P3-CNRS, BP 110, F-74941 Annecy-le-Vieux CEDEX, France
 - 5 Johns Hopkins University, Baltimore, MD 21218, USA
 - 6 Institute of Physics, University of Basel, CH-4056 Basel, Switzerland
 - 7 Institute of High Energy Physics, IHEP, 100039 Beijing, China[△]
 - 8 Humboldt University, D-10099 Berlin, FRG[§]
 - 9 University of Bologna and INFN-Sezione di Bologna, I-40126 Bologna, Italy
 - 10 Tata Institute of Fundamental Research, Bombay 400 005, India
 - 11 Boston University, Boston, MA 02215, USA
 - 12 Northeastern University, Boston, MA 02115, USA
 - 13 Institute of Atomic Physics and University of Bucharest, R-76900 Bucharest, Romania
 - 14 Central Research Institute for Physics of the Hungarian Academy of Sciences, H-1525 Budapest 114, Hungary[‡]
 - 15 Harvard University, Cambridge, MA 02139, USA
 - 16 Massachusetts Institute of Technology, Cambridge, MA 02139, USA
 - 17 INFN Sezione di Firenze and University of Florence, I-50125 Florence, Italy
 - 18 European Laboratory for Particle Physics, CERN, CH-1211 Geneva 23, Switzerland
 - 19 World Laboratory, FBLJA Project, CH-1211 Geneva 23, Switzerland
 - 20 University of Geneva, CH-1211 Geneva 4, Switzerland
 - 21 Chinese University of Science and Technology, USTC, Hefei, Anhui 230 029, China[△]
 - 22 SEFT, Research Institute for High Energy Physics, P.O. Box 9, SF-00014 Helsinki, Finland
 - 23 University of Lausanne, CH-1015 Lausanne, Switzerland
 - 24 INFN-Sezione di Lecce and Università Degli Studi di Lecce, I-73100 Lecce, Italy
 - 25 Los Alamos National Laboratory, Los Alamos, NM 87544, USA
 - 26 Institut de Physique Nucléaire de Lyon, IN2P3-CNRS, Université Claude Bernard, F-69622 Villeurbanne, France
 - 27 Centro de Investigaciones Energeticas, Medioambientales y Tecnologicas, CIEMAT, E-28040 Madrid, Spain[‡]
 - 28 INFN-Sezione di Milano, I-20133 Milan, Italy
 - 29 Institute of Theoretical and Experimental Physics, ITEP, Moscow, Russia
 - 30 INFN-Sezione di Napoli and University of Naples, I-80125 Naples, Italy
 - 31 Department of Natural Sciences, University of Cyprus, Nicosia, Cyprus
 - 32 University of Nijmegen and NIKHEF, NL-6525 ED Nijmegen, The Netherlands
 - 33 Oak Ridge National Laboratory, Oak Ridge, TN 37831, USA
 - 34 California Institute of Technology, Pasadena, CA 91125, USA
 - 35 INFN-Sezione di Perugia and Università Degli Studi di Perugia, I-06100 Perugia, Italy
 - 36 Carnegie Mellon University, Pittsburgh, PA 15213, USA
 - 37 Princeton University, Princeton, NJ 08544, USA
 - 38 INFN-Sezione di Roma and University of Rome, "La Sapienza", I-00185 Rome, Italy
 - 39 Nuclear Physics Institute, St. Petersburg, Russia
 - 40 University and INFN, Salerno, I-84100 Salerno, Italy
 - 41 University of California, San Diego, CA 92093, USA
 - 42 Dept. de Fisica de Partículas Elementales, Univ. de Santiago, E-15706 Santiago de Compostela, Spain
 - 43 Bulgarian Academy of Sciences, Central Lab. of Mechatronics and Instrumentation, BU-1113 Sofia, Bulgaria
 - 44 Center for High Energy Physics, Korea Adv. Inst. of Sciences and Technology, 305-701 Taejeon, Republic of Korea
 - 45 University of Alabama, Tuscaloosa, AL 35486, USA
 - 46 Utrecht University and NIKHEF, NL-3584 CB Utrecht, The Netherlands
 - 47 Purdue University, West Lafayette, IN 47907, USA
 - 48 Paul Scherrer Institut, PSI, CH-5232 Villigen, Switzerland
 - 49 DESY-Institut für Hochenergiephysik, D-15738 Zeuthen, FRG
 - 50 Eidgenössische Technische Hochschule, ETH Zürich, CH-8093 Zürich, Switzerland
 - 51 University of Hamburg, D-22761 Hamburg, FRG
 - 52 High Energy Physics Group, Taiwan, China
- [§] Supported by the German Bundesministerium für Bildung, Wissenschaft, Forschung und Technologie
[‡] Supported by the Hungarian OTKA fund under contract numbers T14459 and T24011.
[‡] Supported also by the Comisión Interministerial de Ciencia y Tecnología
[‡] Also supported by CONICET and Universidad Nacional de La Plata, CC 67, 1900 La Plata, Argentina
[△] Also supported by Panjab University, Chandigarh-160014, India
[△] Supported by the National Natural Science Foundation of China.

$\sqrt{s'}$ (GeV)	30 – 50	50 – 60	60 – 70	70 – 80	80 – 84	84 – 86
Initial Number of Events	5660	6205	11004	28348	36377	38452
Initial Purity (%)	20.9	17.1	19.2	11.8	5.9	4.3
Local Isolation Angle (α_{LI})	15°	15°	15°	15°	21°	24°
Jet Isolation Angle (α_{JI})	20°	20°	20°	20°	21°	24°
Selection Efficiency (%)	48.3	41.0	35.2	29.9	27.4	27.5
Background Scale Factor (MC)	1.69 ± 0.11	1.73 ± 0.13	1.17 ± 0.08	1.42 ± 0.06	1.88 ± 0.08	2.00 ± 0.09
Rescaled Hadronic Background (%)	29.3	19.2	11.6	9.2	7.7	11.6
$\tau^+\tau^-$ Background (%)	2.1	2.6	2.3	1.8	1.6	1.3
Two-photon Background (%)	0.2	0.2	0.1	< 0.1	0.2	0.1
Final Number of Events	1247	1047	1575	2938	2091	1607
Final Purity (%)	68.4	78.0	86.0	89.0	90.5	87.0

Table 1: Summary of the event selection criteria, efficiencies and the background estimation for each reduced centre-of-mass energy interval.

$\sqrt{s'}$ (GeV)	$\langle T \rangle$	$\langle \rho \rangle$	$\langle B_T \rangle$	$\langle B_W \rangle$
30 – 50	$0.903 \pm 0.002 \pm 0.005$	$0.075 \pm 0.002 \pm 0.005$	$0.140 \pm 0.002 \pm 0.005$	$0.090 \pm 0.002 \pm 0.005$
50 – 60	$0.919 \pm 0.002 \pm 0.005$	$0.063 \pm 0.002 \pm 0.003$	$0.122 \pm 0.002 \pm 0.006$	$0.080 \pm 0.002 \pm 0.005$
60 – 70	$0.920 \pm 0.002 \pm 0.004$	$0.060 \pm 0.001 \pm 0.003$	$0.121 \pm 0.002 \pm 0.006$	$0.081 \pm 0.001 \pm 0.005$
70 – 80	$0.927 \pm 0.001 \pm 0.005$	$0.056 \pm 0.001 \pm 0.003$	$0.116 \pm 0.001 \pm 0.006$	$0.076 \pm 0.001 \pm 0.006$
80 – 84	$0.930 \pm 0.001 \pm 0.004$	$0.055 \pm 0.001 \pm 0.004$	$0.112 \pm 0.001 \pm 0.006$	$0.076 \pm 0.001 \pm 0.005$
84 – 86	$0.931 \pm 0.002 \pm 0.003$	$0.054 \pm 0.001 \pm 0.004$	$0.110 \pm 0.002 \pm 0.004$	$0.075 \pm 0.001 \pm 0.006$

Table 2: Mean values of the thrust (T), scaled heavy jet mass (ρ), total jet broadening (B_T) and wide jet broadening (B_W) measured at the six different $\sqrt{s'}$ intervals. The first error is statistical and the second is systematic.

Variable	Fit range	Maximum range
$(1 - T)$	0.025 – 0.250	0.0 – 0.5
ρ	0.015 – 0.252	0.0 – 0.5
B_T	0.000 – 0.250	0.0 – 0.4
B_W	0.030 – 0.200	0.0 – 0.4

Table 3: Ranges used for the QCD fits to the data.

$\sqrt{s'}$ (GeV)		$(1 - T)$	ρ	B_T	B_W
50 – 60	α_s	0.130	0.128	0.130	0.116
	$\chi^2/\text{d.o.f.}$	6.1/7	4.4/10	4.2/6	1.3/6
	Statistical error	± 0.005	± 0.005	± 0.004	± 0.005
	Systematic error	± 0.005	± 0.005	± 0.006	± 0.006
	Overall experimental error	± 0.007	± 0.007	± 0.007	± 0.008
	Fragmentation Model	± 0.011	± 0.003	± 0.006	± 0.004
	Model parameters	± 0.002	± 0.003	± 0.003	± 0.002
	Hadronisation uncertainty	± 0.011	± 0.003	± 0.006	± 0.004
	QCD scale uncertainty	± 0.007	± 0.006	± 0.008	± 0.005
	Matching scheme uncertainty	± 0.005	± 0.003	± 0.005	± 0.008
84 – 86	α_s	0.121	0.111	0.124	0.107
	$\chi^2/\text{d.o.f.}$	2.6/7	5.1/10	6.5/6	3.1/6
	Statistical error	± 0.005	± 0.003	± 0.003	± 0.003
	Systematic error	± 0.004	± 0.005	± 0.006	± 0.006
	Overall experimental error	± 0.006	± 0.006	± 0.007	± 0.007
	Fragmentation Model	± 0.008	± 0.005	± 0.006	± 0.004
	Model parameters	± 0.004	± 0.001	± 0.001	± 0.002
	Hadronisation uncertainty	± 0.008	± 0.005	± 0.006	± 0.004
	QCD scale uncertainty	± 0.005	± 0.003	± 0.007	± 0.003
	Matching scheme uncertainty	± 0.005	± 0.003	± 0.006	± 0.008
	Error due to higher orders	± 0.005	± 0.003	± 0.007	± 0.008
	Overall theoretical error	± 0.009	± 0.006	± 0.009	± 0.009

Table 4: Measured values of α_s at $\sqrt{s'} = 50 - 60$ GeV and $84 - 86$ GeV from the fits to the four event shape variables, the $\chi^2/\text{d.o.f.}$ of the fit and the experimental and theoretical errors.

$\sqrt{s'} \text{ (GeV)}$	$\langle\sqrt{s'}\rangle \text{ (GeV)}$	$\alpha_s (\langle\sqrt{s'}\rangle)$	$\Delta\alpha_s \text{ (experimental)}$	$\Delta\alpha_s \text{ (theoretical)}$
30 – 50	41.2	0.140	± 0.006	± 0.011
50 – 60	55.3	0.126	± 0.007	± 0.010
60 – 70	65.4	0.134	± 0.006	± 0.009
70 – 80	75.7	0.121	± 0.006	± 0.009
80 – 84	82.3	0.120	± 0.006	± 0.009
84 – 86	85.1	0.116	± 0.007	± 0.008

Table 5: Combined α_s at the six centre-of-mass energies from the fits to the four event shape variables and the associated experimental and theoretical errors. The second column gives the average centre-of-mass energy ($\langle\sqrt{s'}\rangle$).

$\sqrt{s} \text{ (GeV)}$	$\alpha_s(m_Z)$
41.2	0.122 ± 0.005
55.3	0.117 ± 0.006
65.4	0.127 ± 0.005
75.7	0.118 ± 0.006
82.3	0.118 ± 0.006
85.1	0.115 ± 0.007
91.2	0.122 ± 0.002
133	0.113 ± 0.006
161	0.111 ± 0.006
172	0.114 ± 0.007
Fitted value	0.1207 ± 0.0016

Table 6: The measured α_s values at different centre-of-mass energies evolved to the m_Z scale. The quoted errors are experimental only.

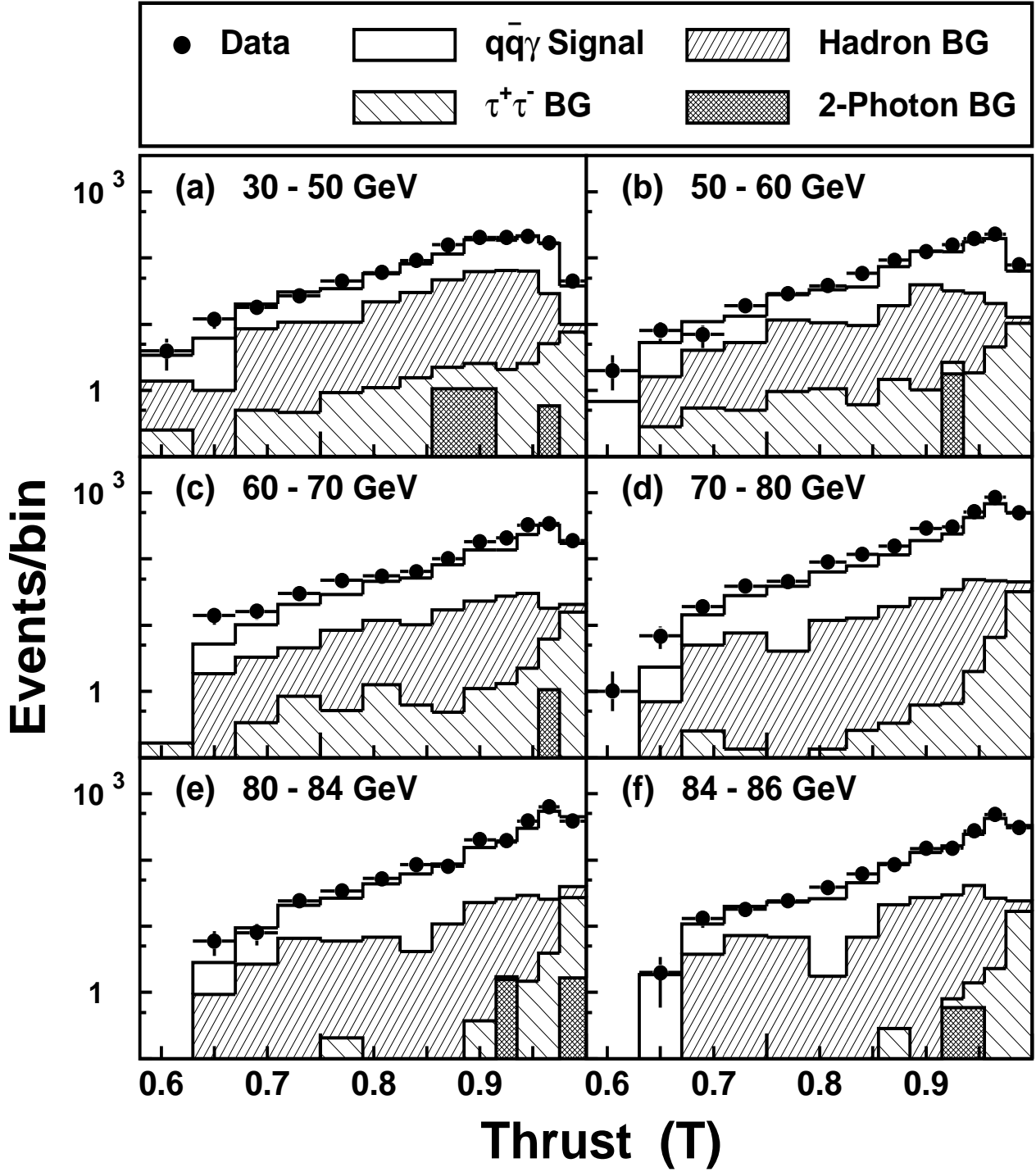


Figure 1: Measured thrust distributions at different reduced centre-of-mass energies (a-f). The solid lines correspond to the overall expectations from theory. The shaded areas refer to different backgrounds and the open area refers to the signal predicted by JETSET. Note that the histograms have a variable bin width.

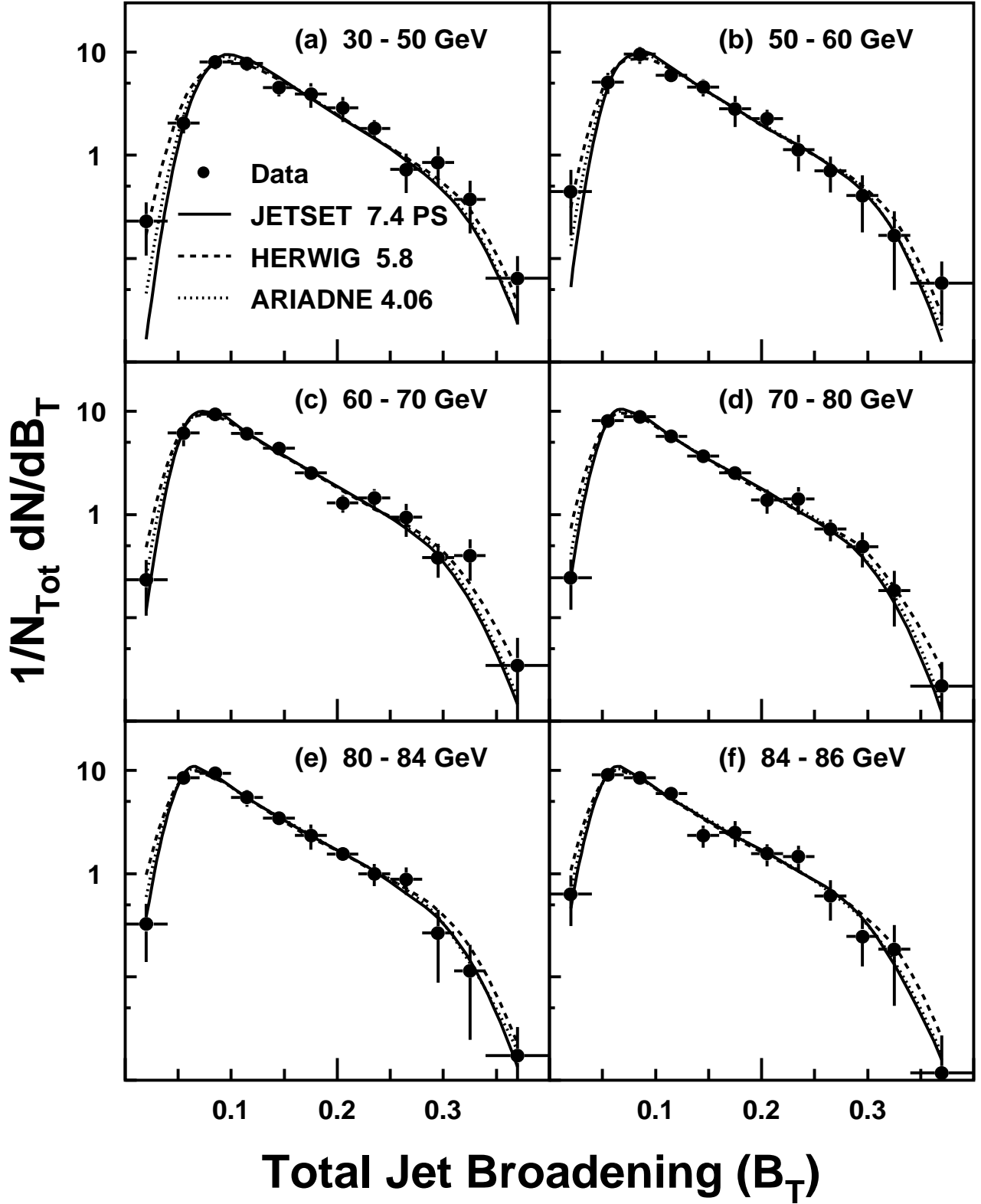


Figure 2: Corrected total jet broadening distributions at different reduced centre-of-mass energies (a-f). The lines correspond to the predictions of different QCD models.

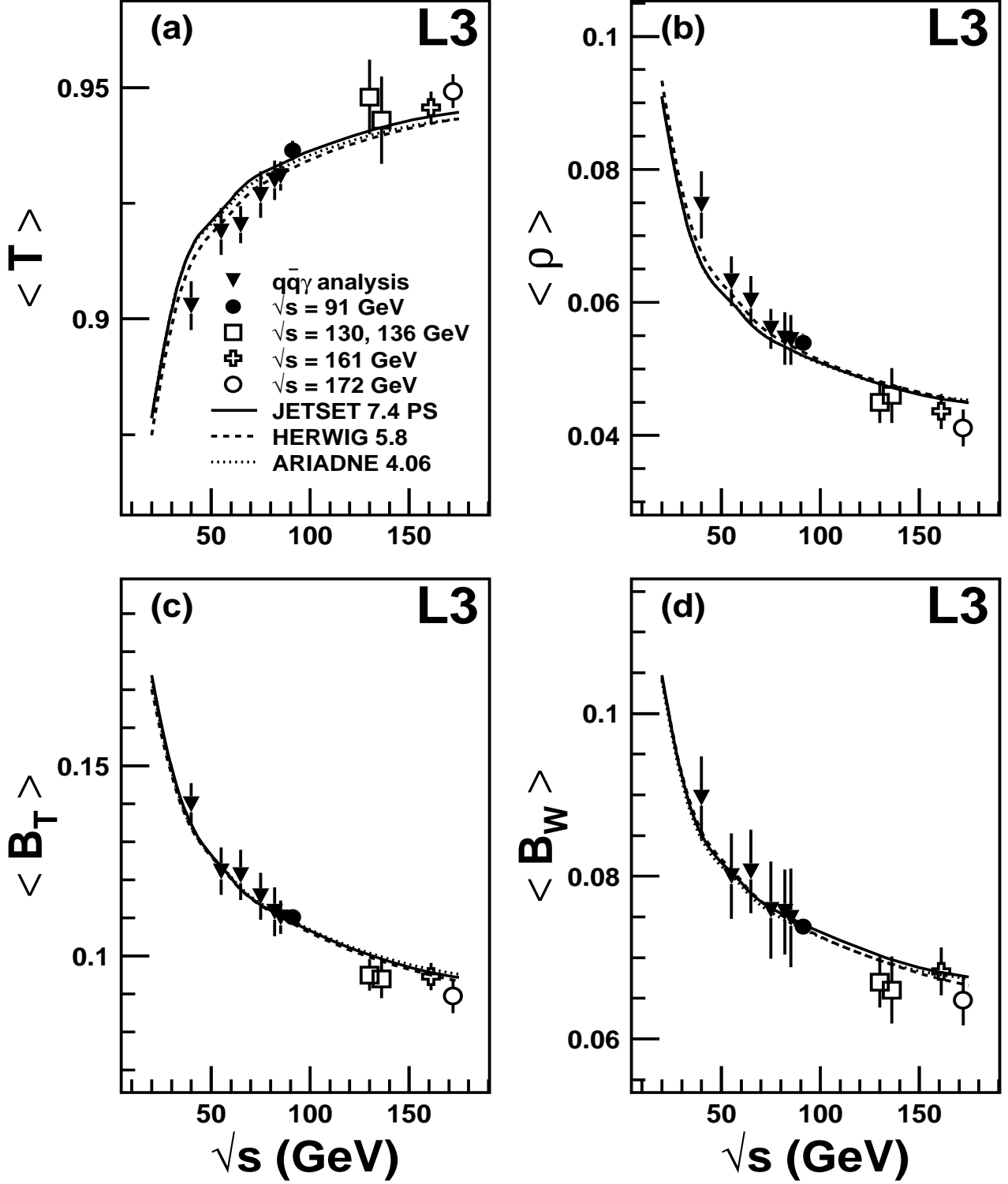


Figure 3: Distributions for the mean values of (a) thrust (T), (b) scaled heavy jet mass (ρ), (c) total jet broadening (B_T), and (d) wide jet broadening (B_W) as a function of centre-of-mass energy. The results of the analysis presented here are compared with our measurements at and above the Z peak. The lines correspond to the predictions of various QCD models.

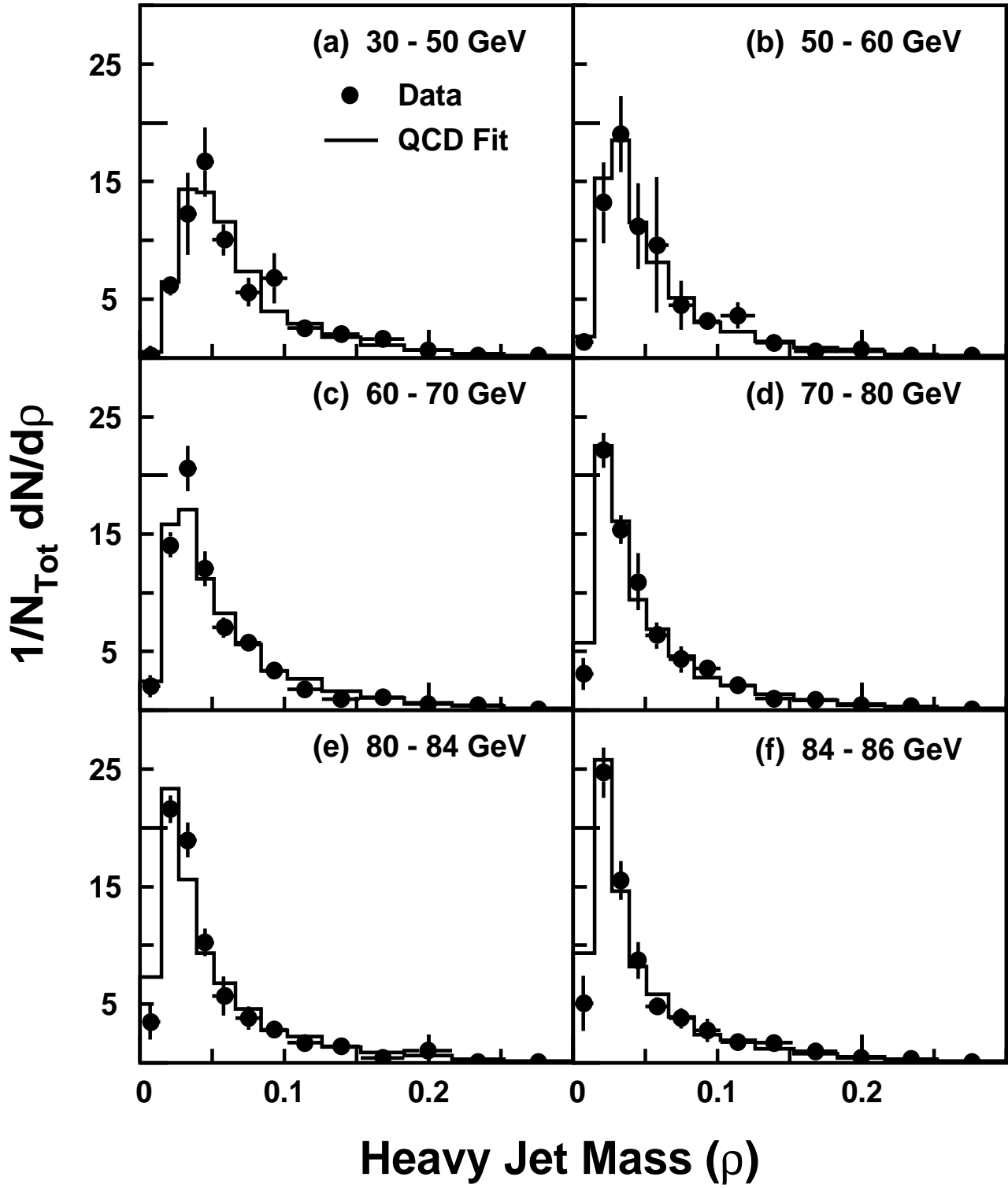


Figure 4: Corrected scaled heavy jet mass (ρ) distributions at different reduced centre-of-mass energies (a-f). The histograms are the fitted QCD distributions.

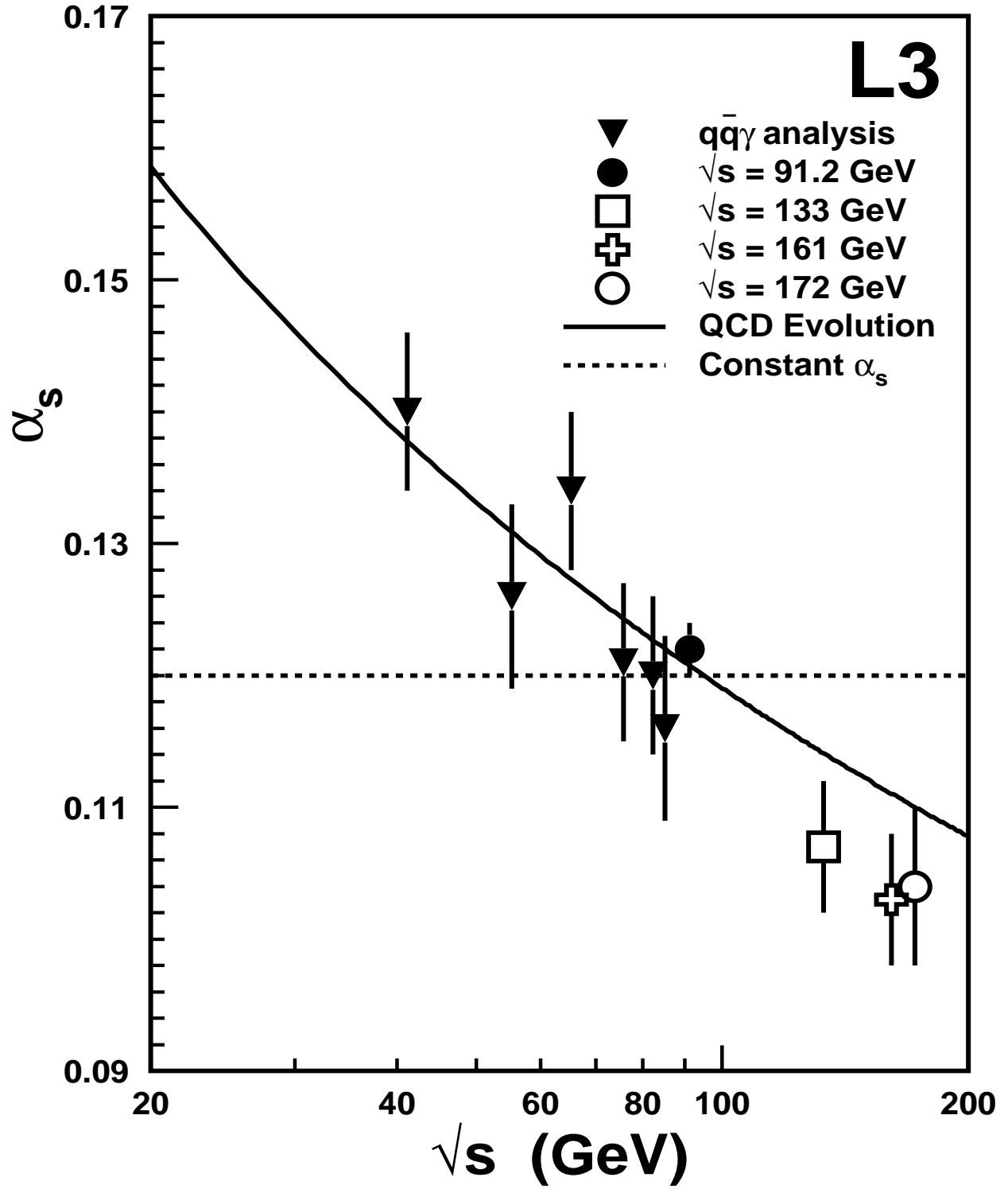


Figure 5: Measured values of α_s from the event shape distributions as a function of centre-of-mass energy. The errors correspond to the experimental uncertainties only. The solid and dashed lines are fits with the energy dependence of α_s as given by QCD and with a constant α_s , respectively.